FRICTION STIR SPOT WELDS BETWEEN ALUMINIUM AND STEEL AUTOMOTIVE SHEETS: INFLUENCE OF WELDING PARAMETERS ON MECHANICAL PROPERTIES AND MICROSTRUCTURE






G. Figner **R. Vallant** **T. Weinberger** **H. Schröttner** **H. Paśič** **N. Enzinger**

ABSTRACT

Hybrid configurations between aluminium and steel are needed to meet today's requirements for lightweight construction in the automotive industry. Different studies showed that Friction Stir Welding (FSW) as well as Friction Stir Spot Welding (FSSW) processes are suitable for joining aluminium to steel. In this work, dissimilar FSSW of aluminium AA5754 and galvanised steel HX 340LAD were examined. In particular the influence of different spindle speeds and dwell times on microstructure and the mechanical properties of the weld were analysed. In doing so, the cross-section microstructure of the weld interface was observed by light optical microscope (LOM) and scanning electron microscope (SEM). The strength of the welds was evaluated both by tensile shear and vibration fatigue tests. The influences of the individual parameters on the weld are presented in detail. The appearance of intermetallic phases (IMPs), a severe problem for conventional fusion welding processes between aluminium and steel, were investigated for the welded samples and a link to the mechanical properties is given.

IIW-Thesaurus keywords: *Aluminium; Friction stir welding; Friction welding; Galvanised steels; Hardness tests; Intermetallics; Lap joints; Light metals; Mechanical properties; Mechanical tests; Microstructure; Process conditions; Process parameters; Reference lists; Steels; Zinc.*

M.Sc. Gunter FIGNER (gunter.figner@tugraz.at), Dr. Rudolf VALLANT (rudolf.vallant@tugraz.at), M.Sc. Thomas WEINBERGER (thomas.weinberger@tugraz.at), and Dr. Norbert ENZINGER (norbert.enzinger@tugraz.at) are with the Institute for Materials Science and Welding, Graz University of Technology, Graz (Austria). Hartmuth SCHRÖTTNER (hartmuth.schroettner@felmi-zfe.at) is with the Research Institute for Electron Microscopy and Fine Structure Research, Graz University of Technology, Graz (Austria), and Haris PAŚIČ (haris.pasic@magnasteyr.com) is with MAGNA STEYR Fahrzeugtechnik AG & Co KG (Austria).

Doc. IIW-1925-08 (ex-doc. SC-Auto-020r1-08) recommended for publication by SC-Auto "Select Committee Automotive and Road transport".

1 INTRODUCTION

The joining of steel and aluminium is becoming an important research topic for automobile manufacturers because of recent demands for high strength, light weight hybrid designs, improved acoustics, corrosion resistance, and crash properties. However the joining technologies of these two materials are quite limited by their different physical and chemical properties. In order to avoid the problem of different melting points and to avoid the formation of thick, brittle intermetallic phases (Fe_nAl_m), adhesive bonding is the mainly used joining technology for those kinds of joints in an automotive body shop. This process provides very good results and durability, especially regarding the corrosion

protection of the joint. An alternative way for avoiding the above mentioned difficulties by brazing/ welding of steel with aluminium is the use of a joining process with very well controlled thermal conditions. By minimizing the energy input brittle intermetallic phases (IMPs) are kept as small as possible. Tests with arc welding (TIG, MIG) [1, 2] have shown that the thickness of intermetallic phase has a major influence on the mechanical properties (tensile shear test results and fatigue behaviour) of steel-aluminium joints. The problem of big differences between the melting points of those two materials can be decreased by use of FSSW, considering that the temperature needed for joining lies below solidus temperature of the used aluminium alloy. For that reason FSSW seems to provide very important advantages for dissimilar joints, compared to typical fusion welding processes, [3-5].

2 EXPERIMENTAL PROCEDURE

2.1 Base material

HX340 LAD sheets of steel (hot-dip galvanized 50 g/m²) of 1 mm thickness and aluminium AA5754-H111 of 2 mm thickness were used for this study. The sheets were cut into 60 mm x 100 mm coupons, and were clamped in a lap configuration, where the Al-sheet is placed on top. The overlapping of the Al-sheet was 20 mm. The nominal chemical compositions of AA5754 and HX 340LAD are shown in Table 1. The ultimate tensile strength of the AA5754/HX340LAD base metals was a minimum of 240 MPa and 510 MPa, respectively.

2.2 Tests performed

The spot welds were produced at the friction stir lab at the Graz University of Technology using the MTS I-Stir BR4 friction stir machine. The forces and torque were measured by high accuracy pressure cells and recorded simultaneously during each spot welding operation.

There are 4 stages in the FSSW cycle time: touchdown, plunging, dwelling and retracting. These stages are represented in Figure 1, which plots the measured temperature (solid red line) and force of the tool (dashed blue line) against the joining time. The dot and dash green line represents the plunging depth of the tool. During touchdown, the tool starts to spin and toughs the aluminum surface, which is placed on top in the lap joint configuration. In the second stage, the tool is plunged into the material, which results in an increase in temperature and tool force. The force then increases very rapidly until it peaks, because on the one hand the tool is penetrating the bottom steel sheet on the other hand the tool shoulder touches the surface of the aluminum sheet. When the present plunging depth is reached, dwell time starts. During the dwelling the tool force drops due to the softened material. After dwelling, the tool retracts from the work piece.

In this approach the time from touchdown to retraction was 18 s (using a 3 s dwell time), the peak temperature of 590 °C is reached in the dwelling phase, and the maximum downward force of the tool amounts 8.3 kN at the end of the plunging.

Table 1 – Alloying elements of the aluminium and steel sheets

Material	Element max. Wt [%]							
AA5754 acc. to EN 573-3	**Si**	**Fe**	**Cu**	**Mn**	**Mg**	**Cr**	**Zn**	**Ti**
	0.4	0.4	0.1	0.5	2.6-3.6	0.3	0.2	0.15
HX340 LAD acc. to EN 10292	**C**	**Si**	**Mn**	**P**	**S**	**Al**	**Ti**	**Nb**
	0.1	0.5	1.0	0.025	0.025	0.015	0.15	0.09

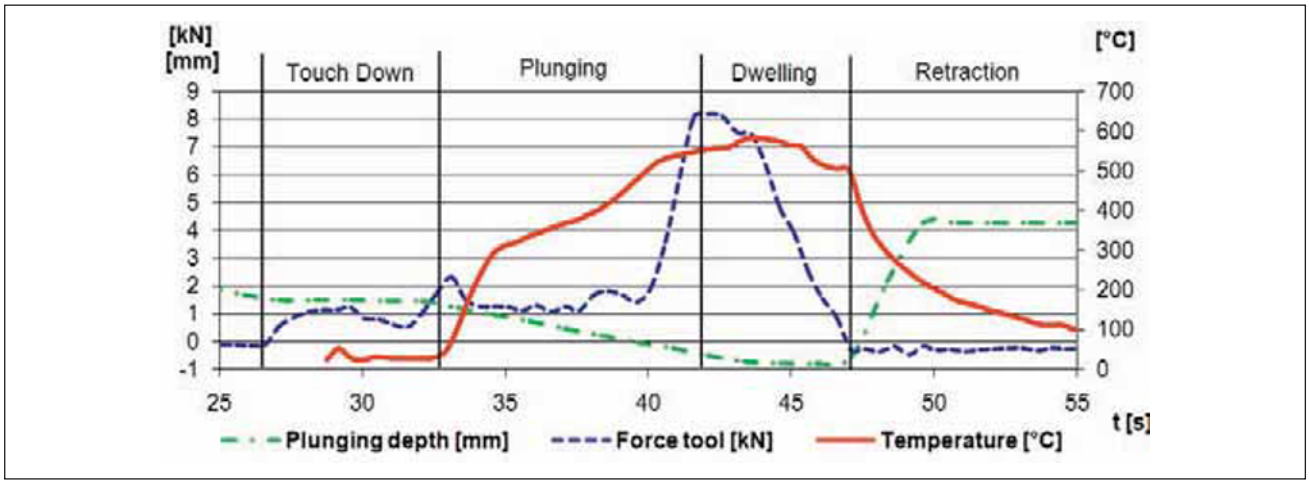

Figure 1 – Principal phases of FSSW

A K-type thermocouple was used to measure the temperature during the friction stir process, and it was fixed to the backside of the steel sheet below the tool pin.

Samples were produced for mechanical testing using a range 0-8 s of dwell times and 800-3 200 rpm spindle speeds. The plunge rate (12 mm/min) and plunge depth (2.2 mm) were constant for all welds. All the welds were made in position control mode. The plunging depth is defined which results in a tool force. A two-piece tool was used for the production of the spot welds. This tool is composed of a cylindrical shaft made of hot work steel AISI H13 with a scrolled shoulder (diameter: 12.7 mm) and a four-flat pin (length: 2.3 mm) of tungsten-rhenium alloy (W25Re).

2.3 Investigations

After producing the welds, the samples were tested using tensile lap shear tests on a tensile testing machine RMC 100®. Four specimens for each parameter set were tested. Altogether, 340 spot welds and 46 parameter sets have been analyzed for this study. Welded samples using the optimized welding parameters were then evaluated using vibration fatigue tests on a resonant testing machine TESTRONIC® (RUMUL), with a minimal load amplitude of 0.75 kN. Testing was aborted when either the sample fractured, defined by a frequency change of more than 10 % or 10 million load cycles were reached. The load ratio R (lower/upper load) was held constant at 0.1.

Etching was performed with hydrofluoric and nitric acid for LOM cross sections. The hardness testing was carried out using EMCOTEST® M1C ecos with a load of 200 g, and the microhardness testing was done using a Paar MHT4 Vickers microhardness tester with a 20 g load and a holding time of 10 s.

SEM images of backscattered electrons (BE) as well as an Angle Selective Backscatter (AsB) were evaluated. The orientation of the steel grains was analyzed by means of Electron Backscatter Diffraction (EBSD). The orientation-angle to different grains was set to 5°.

3 RESULTS AND DISCUSSION

The objective of this work is to compare microstructure and mechanical properties and determine their link to the welding parameters such as rotation speed and dwell time. The welding parameters plunge depth and retraction rate have not been optimized. Hence the cycle time for producing one spot can be greatly reduced.

3.1 Microstructure

Figure 2 shows a macroscopic overview of the cross-section of a dissimilar friction stir spot welded AA5754 alloy to steel HX340LAD. The joint exhibits four distinct regions:

1. base material (BM),
2. heat-affected zone (HAZ),
3. thermo-mechanically affected zone (TMAZ)
4. stirring zone (SZ).

Optical and scanning electron micrographs of these regions are indicated as Figure 3 (details (b, c) of Figure 2) and Figure 4 (details (d, e, f) of Figure 2). For easier classification, the welding parameters spindle speed, dwell time, and the average lap shear strength are inserted in the figures.

Welding tests at 0 s dwell time (just plunging and retraction) show a poor stirring at 1 600 rpm spindle speed, i.e. coarse torn out steel particles in the SZ, Figure 3, detail (b). Applying higher spindle speeds (2 400 rpm) already give much finer particles, resulting in a higher strength of the SZ due to dispersion hardening, Figure 3, detail (c). The average lap shear strength raises from 5.7 kN to 6.5 kN. The raise in the lap shear strength by applying higher spindle speeds could also be explained by increased ligament bonding. Two bonding mechanisms in FSSW aluminum to steel mainly occur: the mechanical clamping via extruded steel and bonding via intermetallics at the interface.

By using higher spindle speeds more heat input is generated enabling more outward spreading of very thin IMPs, which gives higher ligament bonding and higher strength of the joint. In both cases the fracture occurs at the Al -St interface.

Using the SEM with AsB detector, three different zones of the welding were investigated: HAZ, SZ and the zone underneath the exit hole of the pin. The average grain size in the HAZ Figure 4, detail (d) is around 8 µm and gradually decreases by getting closer to the welding centre. In the SZ Figure 4, detail (e) the average grain size is only about 1 µm, and underneath the exit hole Figure 4, detail (f) even less than 1 µm. This is due to the different stresses, deformations, deformation rates and temperatures in the zones. For HAZ, Figure 4,

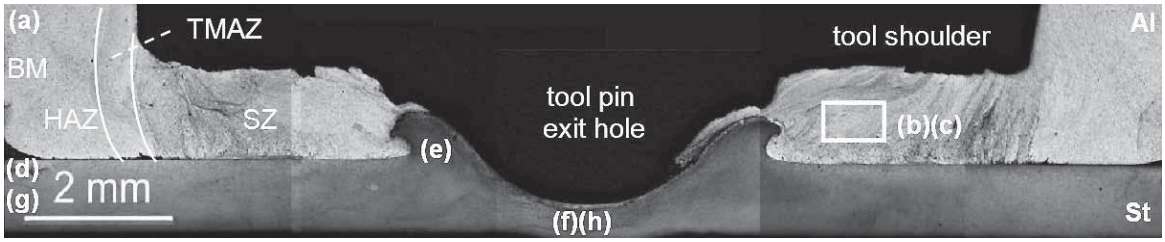

Figure 2 – Microstructure for different weld sites in FSSW

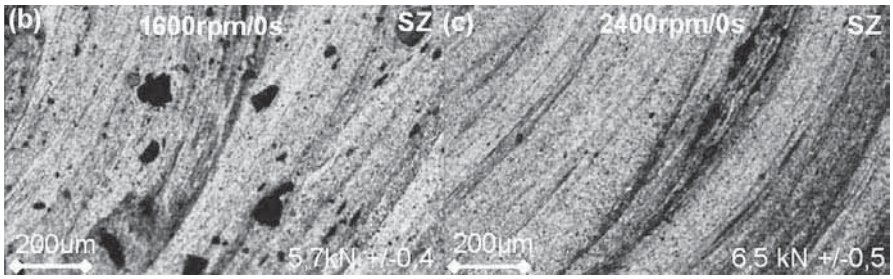

Figure 3 – SZ different spindle speeds – Details (b, c) of Figure 2

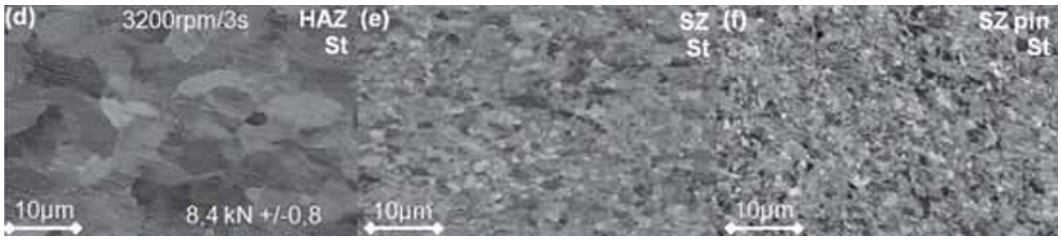

Figure 4 – SEM AsB detector steel – Details (d, e,) of Figure 2

detail (d) the same grain size as in the unaffected steel sheet can be observed, i.e. there is no influence on the microstructure. However for the plastically deformed zones Figure 4, details (e) and (f) a strong grain refinement occurs.

The EBSD analysis of the steel was performed to evaluate the orientation of the grains. The original microstructure of the steel Figure 5, detail (g) is composed of slightly elongated grains with an average diameter of 8 µm; sub-grains were found due to the rolling process. Below the exit hole a recrystallized microstructure of small grains with a diameter < 1 µm was observed, Figure 5 detail (h).

No former austenitic structure was detected during EBSD analyses, which correlates with the measured peak temperature of 590 °C see Figure 1, i. e. below the A1 temperature of steel. The grain refinement is probably caused by dynamic recrystallization, i.e. high deformation rates and temperatures. Finer grains are reformed continuously (steady nucleation and growth), which should be most severe beneath the exit hole. Bozzi *et al.* [6] reported that dynamic recrystallization also occur during the FSSW process on the Al sheet.

3.2 The formation of Intermetallic Phases (IMPs)

The formation of IMPs plays an important role in welding dissimilar materials, especially aluminium to steel. The mechanical properties of a joint are strongly influenced by the composition and by the thickness of the IMPs. Chemical compositions at the interface between the aluminium alloy and steel was estimated by EDXS analysis.

Figure 6 a) shows an overview of a SEM cross section FSSW Al-St. The wave-shape of the steel is formed by the pin rotation as well as the downward forge force of the tool. IMPs are generated at the phase boundaries Figure 7, detail (c), as well as at torn-out steel particles [Figure 6 b), Figure 7, detail (d)] located in the Al-matrix. The quantitative spot analyses of the IMPs result in an estimated composition of 40-42wt% Fe and 58-60 % Al, as can be seen in Figure 7 and Table 2.

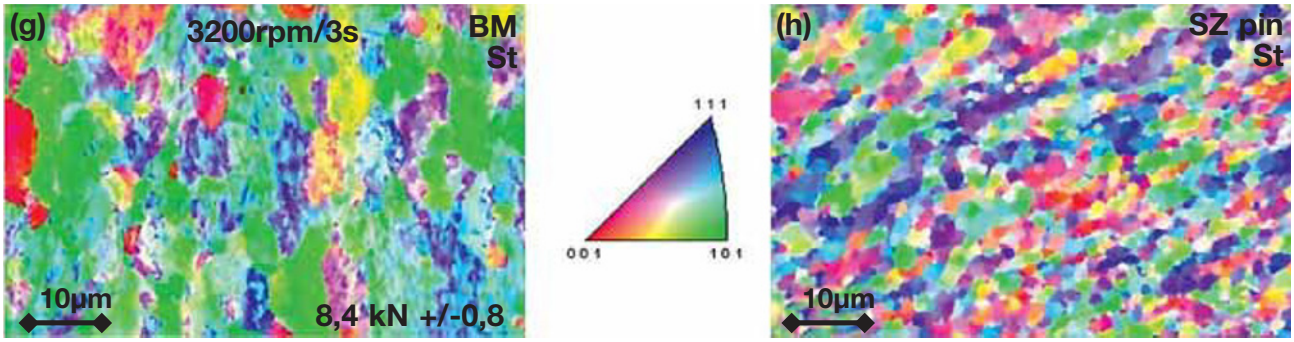

Figure 5 – EBSD steel – Details (g, h) of Figure 2

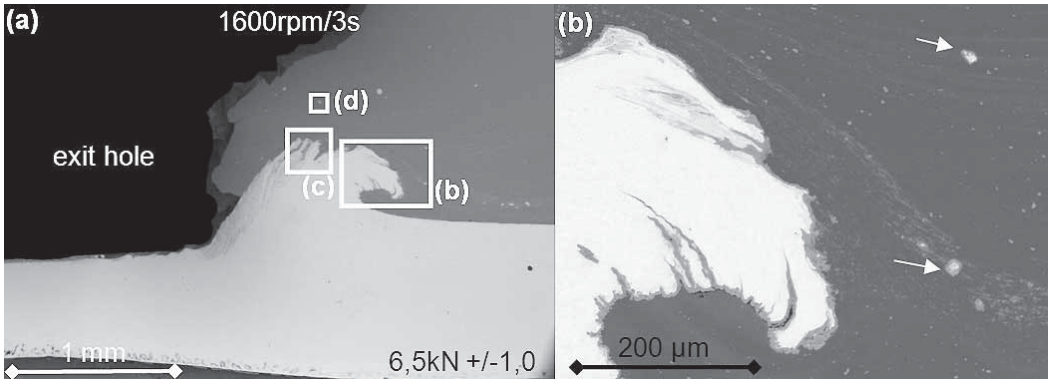

a) SEM overview FSSW cross-section **b) IMPs on steel particle in the aluminium matrix (SZ)**

Figure 6

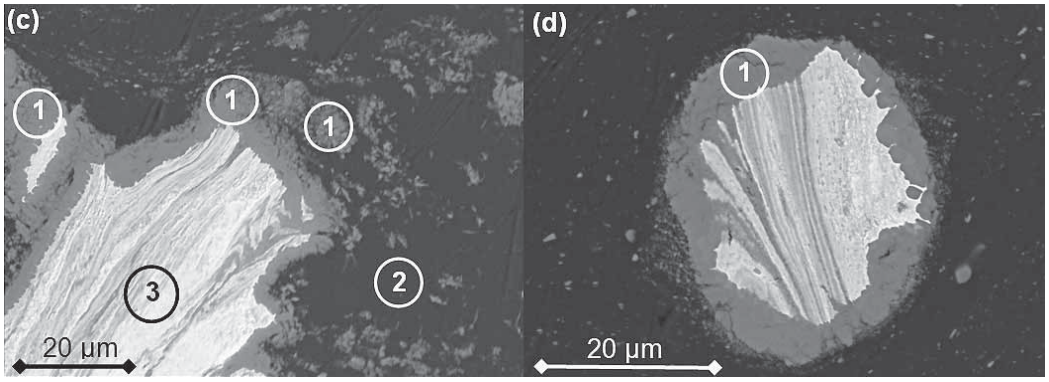

Figure 7 – IMPs on the wave peak (SZ) – Details (c, d) of Figure 6

Table 2 – EDXS spot analysis – approx. element concentrations – Details of Figure 7

Figure	EDXS spot No.	Element	Wt %	Phase
7 (c)	1	Al	59	Fe_2Al_5
		Fe	40	
	2	Al	~99	Al-Matrix
		Fe	<1	
		Mg	<1	
	3	Al	29	Steel matrix with diffusion paths
		Fe	70	
		Mn	1	
7 (d)	1	Al	58	Fe_2Al_5
		Fe	42	

According to the phase diagram in the binary Fe-Al system, [7] $FeAl_3$ and Fe_2Al_5 should appear as stable IMPs. Different investigators reported that at low temperatures (< 700 °C) only Fe_2Al_5 is produced at the Fe/Al interface [8-11]. If the materials are deformed, the plastic deformation enforces diffusion; according to Naoi *et al*. [9] and Heumann *et al*. [12] the formation of Fe_2Al_5 starts earlier at 400 °C. In case of FSSW high plastic deformation is created due to the tool stirring action. Temperature measurements at the welding centre result in 590 °C (Figure 1), so the temperatures in the SZ are probably higher than 400 °C.

At the strongly deformed areas of the steel wave (Figure 7 detail (d) EDXS spot 3, Table 2), a high amount of approx. 30 wt% Al is found, i.e. fast diffusion paths for aluminium are present. This might be due to the high density of defects in the Fe-lattice as well as the high vacancy diffusion of Al in the formed orthorhombic lattice of the Fe_2Al_5 [12].

The welding parameter dwell time influences the layer thickness of the created IMPs and thereby the mechanical properties of the spot weld. For this reason the thickness of the IMPs are investigated in different regions of the Fe/Al interface which are marked in Figure 8:

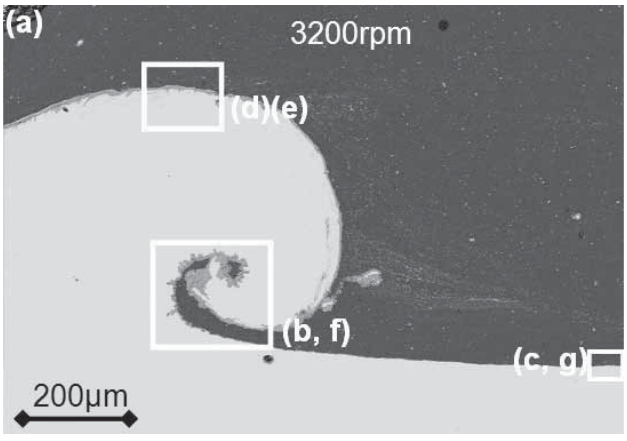

Figure 8 – SEM overview FSSW cross-section, IMP layers

the wave top, the wave centre and in the SZ approx. 0.5 mm away from the wave peak.

The layer thickness for optimized parameters (3 200 rpm and 3 s dwell time) is in the range of 30 µm wave centre, Figure 9 detail (b), and around 1 µm in the SZ, Figure 9 detail (c) Frerichs [13] and Zhang *et al*. [2] have shown that for a mechanically sound joint, the thickness of the intermetallic layer has to be less than 10 µm.

Increased dwell time (8 s) at constant spindle speed creates a higher amount of IMPs. Same results are published by Yilmaz *et al.* [14]. However the thickness of the intermetallic layer on the wave top is similar if dwell time is increased; compare Figure 10 details (d) and (e). The IMPs are growing and probably released to the Al-Matrix, i.e. they break off discontinuously after reaching approx. 5 µm. The tensile shear strength is almost halved by increasing the dwell time to 8 s.

In other words the intermetallic layer has the same thickness for a dwell time 8 s as the sample with good mechanical properties. However the strength of the weld is harmed by the additional creation and dispersion of IMPs in the SZ of the Al-matrix.

3.3 The influence of zinc

SEM pictures of FSSW of aluminium to non galvanized steel also show the presence of IMPs. They are also created at the steel wave centre as well as on the wave top. The thickness of the intermetallic layer is nearly the same compared to the Zn coated samples; compare Figure 9 detail (b) and Figure 11 detail (f). However, in the SZ approx. 0.5 mm away from the wave peak no IMPs and therefore no bonding is visible at the interface. IMPs were present at the same position using zinc-coated sheets; compare Figure 9 detail (c) and Figure 11 detail (g). This reduction in bonding results in a reduction of the strength of 30 % in comparison to galvanized steel sheets using optimized welding parameters: 3 200 rpm and 3 s dwell time.

Several EDXS analysis of the IMPs at the Fe/Al interface could not detect any Zn (using Zn-coated steel sheet), although the IMP type Fe_2Al_5 is able to dissolve Zn in quantities (up to 28 wt%) [15, 16]. High Zn-concentrations up to 20 wt% are found only at the edges of SZ of the aluminium sheet, Figure 12 details (a, b). This is probably due to the material flow in the SZ which transports Zn from the Fe/Al interface towards the edge of the SZ. It is assumed that the low melting Zn (melting point: 419 °C) is in liquid state due to the present temperature of 590 °C measured in the welding centre (see Figure 1).

Hence, Zn is not part of the IMP but it strongly influences the formation of IMPs. Schneider *et al.* [17] reported that the addition of zinc accelerates the reaction between iron and aluminium. Zn can probably act

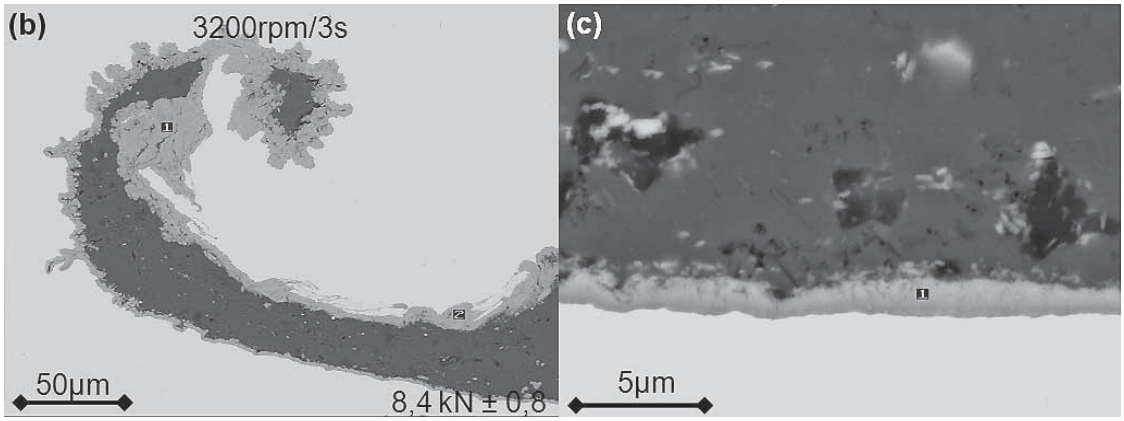

Detail (b) Steel wave centre **Detail (c) Al-St interface SZ**

Figure 9 – Details (b, c) of Figure 8

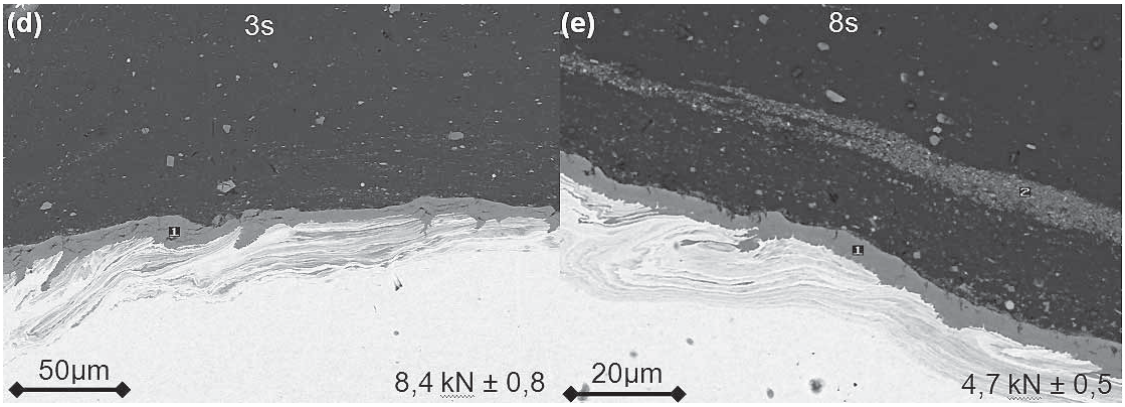

Figure 10 – Details (d, e) of Figure 8: Wave top, distribution of IMPs at 3 and 8 s dwell time

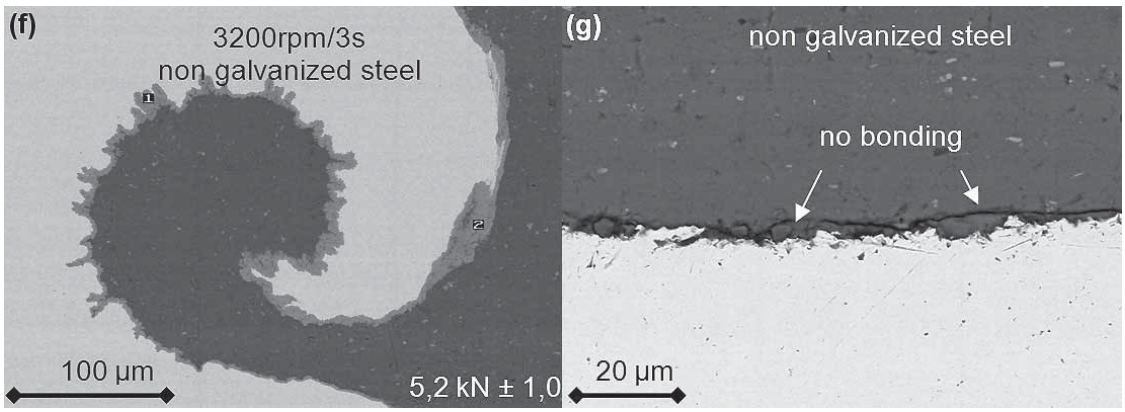

Detail (f) Steel wave centre peak non galvanized steel **Detail (g) Al-St interface SZ non galvanized steel**

Figure 11 – Details (f, g) of Figure 8

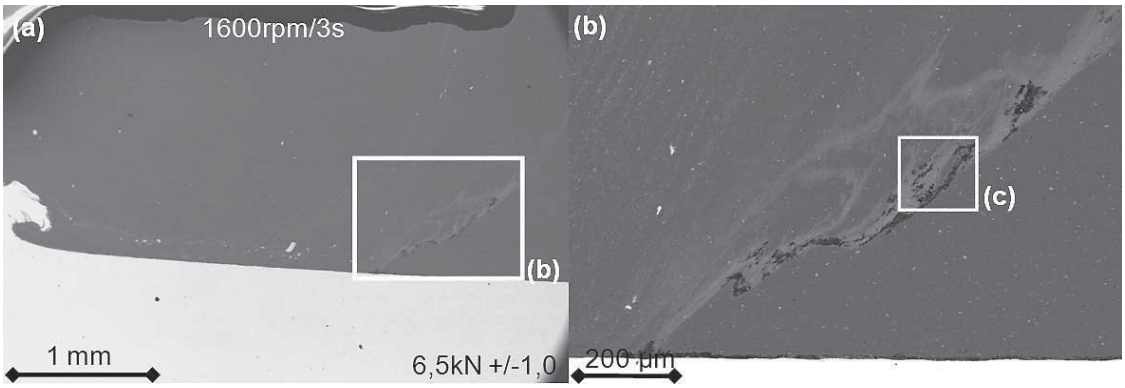

Figure 12 – SEM overview FSSW cross-section – Details (a, b)

as a fluxing agent, dissolving and removing the impurities away from the Al-Steel joint interface. In doing so, a thin and continuous IMP in the SZ can be formed for a good bonding of aluminium to steel.

The encircled numbers in Figure 13 mark the positions of the EDXS-spot analyses summarised in Table 3:

(1) Al-Matrix,

(2) brighter Zn-enriched area,

(3) impurities, as well as

(4) a primary precipitation in the HAZ of Al-plate.

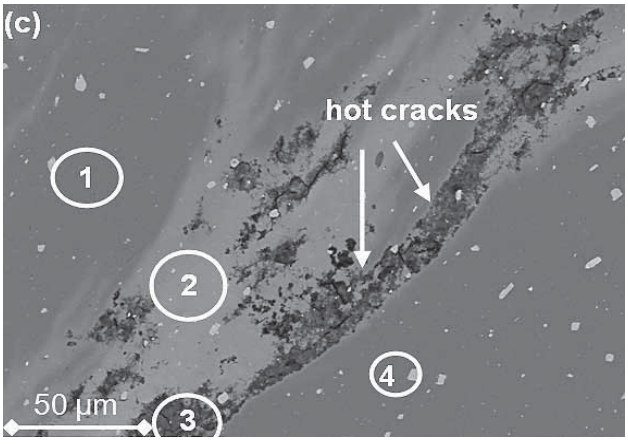

Figure 13 – FSSW cross-section edge SZ Detail (c) of Figure 12

The impurities (3) are of complex alloy elements composition, including O and S. This corresponds to low melting multicomponent phases, which show a wide temperature range for solidification. Therefore in Figure 13 hot cracks in the area of the impurities are visible [18]. As the fracture of the joint for static and dynamic loading is not associated to the appearing hot cracks, they should not be critical.

Table 3 – EDXS spot analysis – approx. element concentrations (details of Figure 13)

EDXS Spot No.	Element	Wt %	Phase
(c) 1	Al	98	Al-matrix
	Mg	2	
(c) 2	Al	82	Al-Zn solid solution area
	Mg	<1	
	Zn	17	
(c) 3	Al, Zn, Mg	-	impurities/ multi-component phase
	Fe, Si, Mn		
	O, S		
(c) 4	Al	61	primary precipitation
	Fe	24	
	Mn	9	
	Si	5	

3.4 Tensile shear strength

Figure 14 a) shows the average tensile shear strength against the dwell time and spindle speed. For each parameter set, four specimens were tested, and the standard deviation was always less than 15 % of the average strength value. Increasing the spindle speed at constant dwell time leads to higher strength. This trend was observed at different spindle speeds. This is clearly visible for 1, 2 and 3 s dwell times. Applying higher spindle speeds leads to fine dispersed particle in weld, see Figure 3 detail (c). For higher dwell times, (5 s, 8 s) this tendency is not clear; some intermediate spindle speeds give higher tensile shear strength. The maximum strength of the weld was achieved at maximum spindle speed (8.3 kN using 3 200 rpm/3 s).

Figure 14 b) shows the fracture surface of the tested tensile shear specimen. For all welds, the fracture occurred at the aluminium/steel interface. Aluminium was found near the exit hole of the tool at the steel fracture surface.

Two distinct modes of failure of FSSW are described in the literature: pullout and interfacial fracture. Pullout failures result in significantly higher energy absorption due to the large displacement prior to separation of the sheets. The mean fracture peak load for static lap shear tests of the nugget pullout mode is slightly higher than for the interfacial fracture for similar joints [19]. All tested welds broke at the aluminium steel interface.

3.5 Fatigue strength

For determining the fatigue strength, test samples of three spots were produced using optimal welding parameters to get the highest static shear strength. Figure 15 a) shows the fatigue strength of 9 FSSW 3-spots-samples. Figures 15 b) and (c) show a FSSW top view as well as cross-section after fatigue failure. It is likely that the fatigue crack is initiated at the interface and propagates through the stirring zone of the aluminium. The existence of pores and gaps at the aluminium/steel interface could have promoted a crack path and initiated the interfacial fracture mode, as shown in Figure 9 detail (c).

3.6 Hardness measurements

For 1 600 rpm spindle speed and 3 s dwell time the distribution of Vickers hardness HV 0.2 was measured in a FSSW cross-section, Figure 16.

The hardness in the aluminium alloy exhibit values from 75 to 78 HV0.2 in the outer stirring zone near to the HAZ and the zone near to the pinhole, respectively. As the hardness of the aluminium base material is 67 HV 0.2 ± 2 a slight hardness increase in the stirred zone towards the centre pin exit hole is observed. This increase could be explained by the fine dispersed steel particle in the aluminium, as shown in Figure 3 detail (c).

Below the pin exit hole the hardness in steel mounts from 210 to 270 HV0.2, the unaffected steel gives values between 151 and 160 HV0.2. At the top of the steel wave the hardness raises up to 360 HV0.2, Figure 16. This hardness increase below the pin exit hole and at the wave top are probably due to high deformation rates and temperatures during welding which leads to grain refinement caused by dynamic recrystallization, as seen in EBSD Figure 5 detail (h).

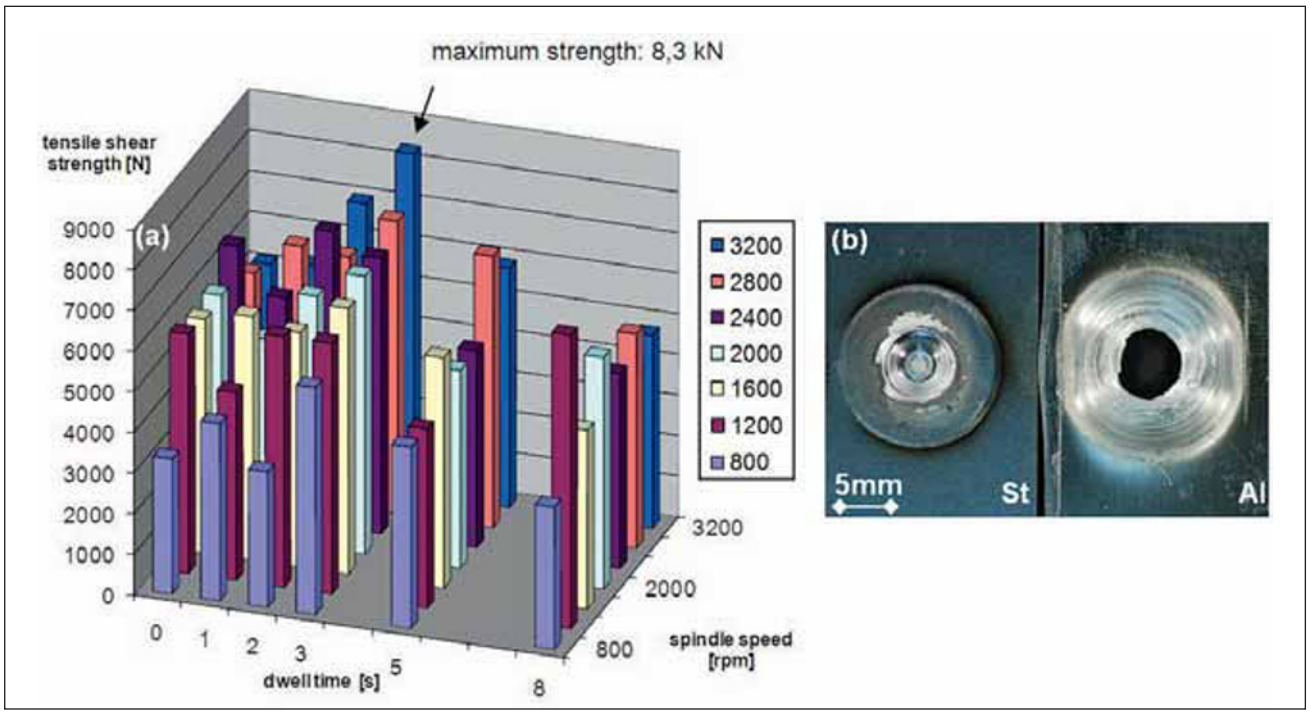

a) Lap shear strength of Al-St FSSW for different spindle speeds and dwell times

b) Top view lap shear sample after breakage

Figure 14

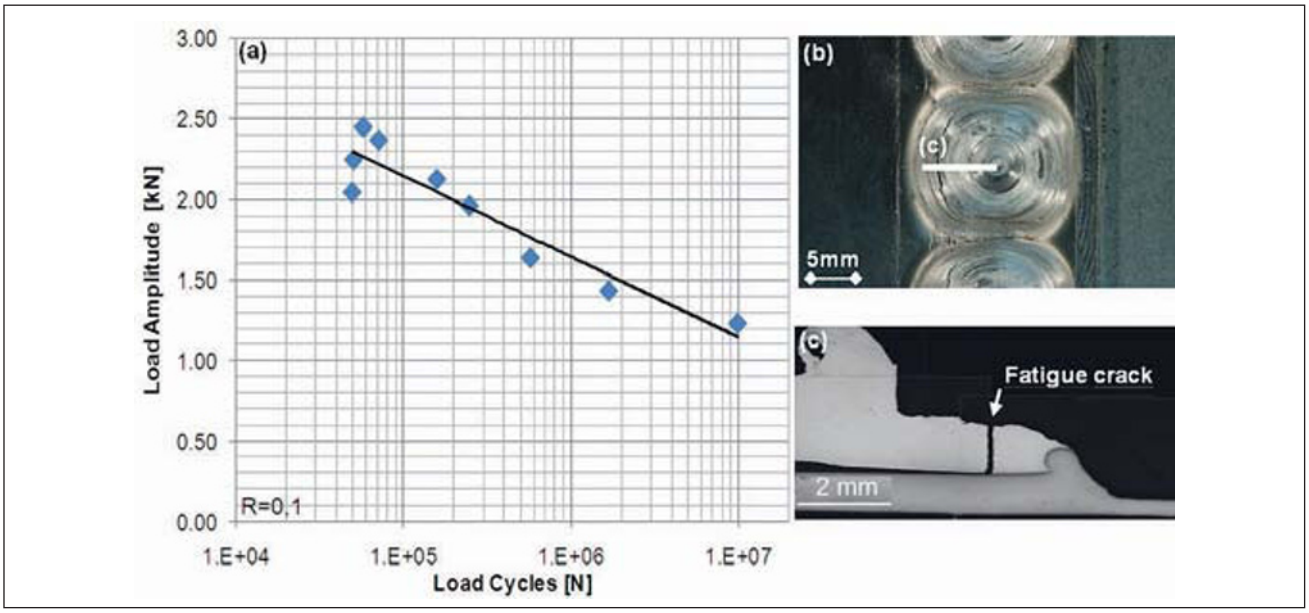

a) Results of vibration fatigue tests of 3-spots-samples
b) Top view fatigue sample after breakage
c) Cross-section fatigue sample

Figure 15

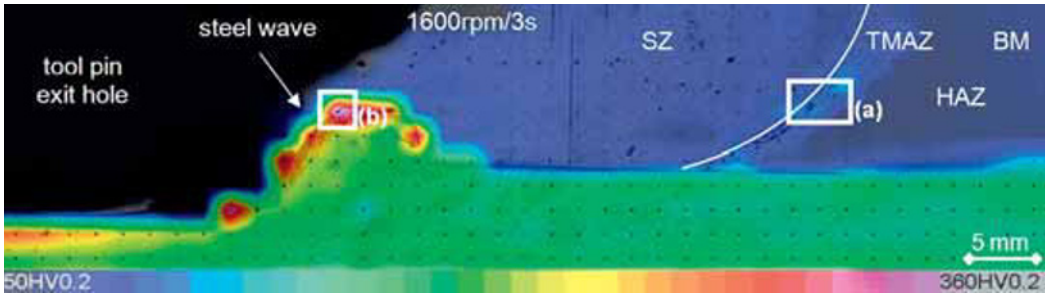

Figure 16 – Distribution of Vickers micro hardness HV 0.2 / FSSW cross-section

The major hardness increase at the border of SZ in aluminium was verified by a micro hardness measurement, Figure 17 a): approx. 130 to 200 HV0.02 were found. This is a significant increase compared to values in the adjacent areas which are 78 and 68 to 72 HV0.02. This raise is probably caused by solid solution hardening by Zn, as shown in Figure 13. At the boundary to the aluminium area almost 500 HV0.02 appear, Figure 17 b). This is probably due to the formation of brittle IMP. Generally IMPs have a high hardness; according to Meyer *et al.* [8] the hardness of IMP Fe_2Al_5 is up to 835 HV0.2. Due to brittleness, IMPs continuously break off at the interface because of high shear stresses in the SZ. The particles are sequentially dispersed in the Al-matrix, as seen in Figure 10 detail (e).

4 CONCLUSIONS

This study investigated the feasibility of FSSW between aluminium and steel sheets. Parameters were optimised with respect to static tensile shear strength. LOM, SEM, hardness, strength and fatigue strength was investigated. It was found that:

1. Using proper selection of spindle speed and dwell time, the strength of the spot weld can be improved significantly. Thus a maximum load in the shear tension test of 8.4 kN per spot can be achieved. By increasing the dwell time the amount of IMPs rises and breaks off, causing a drop in strength. Higher spindle speed causes a fine distribution of steel particles in the stirring zone and leads to higher bearable loads in the shear tension test.

2. AsB (and EBSD) images of the steel show very fine grains below the pin and in the wave. This is due to dynamic recrystallization of the stirring zone. Grains become coarser away from the welding centre.

3. During friction stage, Fe particles from steel were taken into aluminium alloy by mechanical mixing.

4. Layers of intermetallic compounds Fe_2Al_5 were found at the bond interface. The thickness of the layer was between 1 and 30 µm depending on the position.

5. Zinc at the interface improves the bonding via the formation of thin IMPs. Zn is expected to be in the fluid state as it is moved outwards to the edges of the stirring zone, where it was found in higher concentrations.

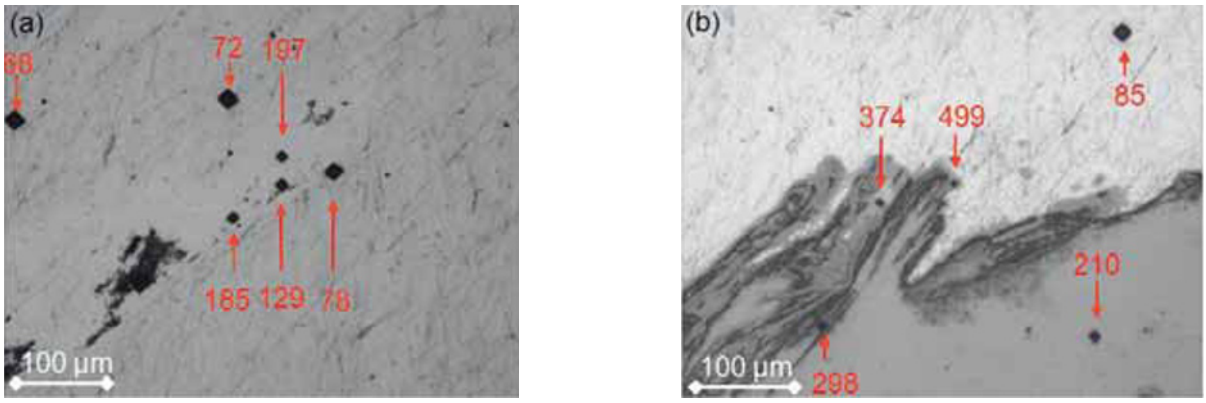

a) at the etches of SZ – detail of Figure 16

b) at the steel wave – detail of Figure 16

Figure 17 – Distribution of Vickers micro hardness HV 0.02

The FSSW process is relatively slow compared to Resistant Spot Welding (RSW). For producing a RSW spot only a split second, for FSSW 18 seconds are needed. In this work the objective was to optimize the welding parameters with respect to mechanical properties. However for the application in automotive production the cycle times have to be further reduced, especially by accomplishing tests with higher penetration speed.

ACKNOWLEDGEMENTS

The authors give thanks to the JOIN – Network of Excellence for Joining under the support of Federal Ministry of Economics and Labour (BMWA) and the project partners MAGNA, Fronius, HAGE, Institute for Forming and High Power Laser Technology, SZA and TU Graz in Austria.

REFERENCES

[1] Resch J.: Untersuchung zur Problematik der Metall-Schutzgassschweißung von Aluminium und Stahl (Construction of diffusion-layers MIG wire electrode welding of unalloyed steel and aluminium), MUL Leoben, 1994.

[2] Zhang H.T., Feng J.C., He P., Hackl H.: Interfacial microstructure and mechanical properties of aluminium-zinc-coated steel joints made by a modified metal inert gas welding-brazing process, Materials Characterization, 2007, Vol. 58, 7, pp. 588-592.

[3] Dupont J.N., Banovic S.W., Marder A.R.: Microstructural Evolution and Weldability of Dissimilar Weld between a Super Austenitic Stainless Steel and Nickel-Based Alloys, Welding Journal, June 2003, pp. 125-S-135-S.

[4] Sato Y.S., Nelson T. W., Sterling C.J., Steel R. J., Pettersson C.O.: Microstructure and mechanical properties of friction stir welded SAF 2507 super duplex stainless steel, Materials Science & Engineering. A, 2005, Vol. 397, No. 1-2, pp. 376-384.

[5] Uzun H. Dalle Donne C., Argagnotto A., Ghidini T., Gambaro C.: Friction stir welding of dissimilar Al 6013-T4 To X5CrNi18-10 stainless steel, Materials & Design, 2005, Vol. 26, No. 1, pp. 41-46.

[6] Bozzi S. et al.: Influence of the dwell time on spot welding between 6008 Al alloy and steel by FSW in Proceedings of the Sixth International Friction Stir Welding Symposium, 2006, Saint Sauveur.

[7] Binary alloy phase diagrams, ASM Handbook, Vol. 03, 1992, Materials Information Society.

[8] Meyer L., Bühler H.-E.: Aufbau von Diffusionsschichten zwischen unlegiertem Stahl und Aluminium (Construction of diffusion-layers of unalloyed steel and aluminium), Aluminium 1967, vol. 12, pp. 733-738.

[9] Naoi D., Kajihara M.: Growth behavior of Fe2Al5 during reactive diffusion between Fe and Al at solid-state temperatures, Materials Science & Engineering: A, 2007, Vol. 459, No. 1-2, pp. 375-382.

[10] Sundaresan S., Murti K.G.K.: The formation of intermetallic phases in aluminium-austenitic stainless steel friction welds, Materials Forum, 1994, Vol. 17, No. 3, pp. 301-307.

[11] Malevskii Y.B. et al.: Effects of the annealing conditions on the phase changes taking place in thin composite aluminium-iron films, Avt. Svarka, 1971, Vol. No. 1, pp. 30-34.

[12] Heumann T., Dittrich S.: Über die Kinetik der Reaktionen von festem und flüssigem Aluminium mit Eisen (Over the kinetics of the reactions of solid and liquid aluminium with iron), Zeitschrift für Metallkunde, 1959, Vol. 50, pp. 617-635.

[13] Frerichs F.: Untersuchungen zum Kirkendall-Effekt im gesamten Konzentrationsbereich von binären Diffusionssystemen (Examinations about the Kirkendall-effect in the entire concentration-area of binary diffusion-systems), 2001.

[14] Yilmaz M., Cöl M., Acet M.: Interface properties of aluminum/steel friction-welded components, Materials Characterization, 2002, Vol. 49, No. 5, pp. 421-429.

[15] Marder A.R.: The metallurgy of zinc-coated steel, Progress in Materials Science, 2000, vol. 45, pp. 191-271.

[16] Köster M., Schuhmacher B., Sommer D.: The influence of the zinc content on the lattice constants and structure of the intermetallic compound Fe2Al5, Steel Research, 2001, vol. 72, No. 9, pp. 371-375.

[17] Scheider K., Kessler H.: Die Reaktion von festem Eisen mit Schmelzen zinkhaltiger Aluminiumlegierungen (The reaction of solid iron with meltdowns of zinc-containing aluminum-alloys), Metall, 1953, vol. 7, 15/16, pp. 608-618.

[18] Achar D.R.G. et al.: Verbinden von Aluminium mit Stahl besonders durch Schweißen (III) (Connecting aluminum to steel particularly through welding (III)), Aluminium, 1980, vol. 56, 4, pp. 291-293.

[19] Sun X., Stephens E.V., Khaleel M.A., Shao H., Kimchi M.: Resistance spot welding of aluminium alloy to steel with transition material – From process to performance – Part I: Experimental study, Welding Journal, June 2004, pp. 188-S-195-S.